

Genesis of the periodic lattice distortions in the charge density wave state of $2H$ -TaSe₂Valeri Petkov ^{1,*}, Kamal Chapagain ¹, Sarvjit Shastri,² and Yang Ren²¹*Department of Physics, Central Michigan University, Mt. Pleasant, Michigan 48858, USA*²*X-ray Science Division, Advanced Photon Source, Argonne National Laboratory, Argonne, Illinois 60439, USA*

(Received 5 January 2020; revised manuscript received 9 March 2020; accepted 10 March 2020; published 19 March 2020)

Using high-energy x-ray diffraction and large-scale three-dimensional structure modeling, we reveal the evolution of local lattice distortions in the archetypal charge density wave (CDW) system $2H$ -TaSe₂ as it is cooled from its normal state above room temperature down to temperature where Ta atoms form a long-range ordered superstructure. In particular, we find that the structure is formed via a gradual in-plane clustering of Ta atoms exhibiting unusually short bonding distances already near room temperature, and not via a cooperative distortion of Ta atomic planes taking place at the critical ordering temperature. Our findings clarify the debated local symmetry and magnitude of the periodic lattice distortions in the CDW state of $2H$ -TaSe₂, and emphasize the role of locally correlated lattice distortions as a precursor of CDWs in low-dimensional solids. Also, we demonstrate an efficient experimental approach to study them.

DOI: [10.1103/PhysRevB.101.121114](https://doi.org/10.1103/PhysRevB.101.121114)

Charge density waves (CDWs) in low-dimensional solids are a subject of extensive research due to their relevance to fascinating quantum phenomena such as superconductivity. Also, they hold promise for practical applications in the fields of ultrafast electronics and optics. Currently, the CDW state is understood as a long-range modulation of the electron density coupled to a periodic distortion of the crystal lattice (PLD) emerging below a critical ordering temperature, T_{CDW} [1–7]. While PLDs in the regime of both weak- and strong-coupling CDWs are well studied, little is known about the nature of lattice distortions above T_{CDW} , and their relationship to the PLDs below T_{CDW} . This is because lattice distortions related to CDWs are largely studied by imaging and crystallographic techniques that are difficult to apply when the distortions are less well defined or not perfectly periodic, as they usually are above T_{CDW} [8–11]. Here we use experimental techniques that are applicable to systems with any degree of structural distortions and periodicity to study the evolution of lattice distortions in the archetypal CDW system $2H$ -TaSe₂ over a broad temperature range. We find that lattice distortions in this system appear as unusually short Ta-Ta bonding distances already near room temperature. The distances fluctuate due to thermal excitations but become increasingly correlated locally with decreasing temperature, reflecting the formation of small clusters of Ta atoms characteristic to the CDW/PLD state of $2H$ -TaSe₂ well before it emerges. The clusters are well separated from each other above T_{CDW} and merely form a superstructure when T_{CDW} is reached. Our observation of persistent Ta clustering above T_{CDW} indicates that the long-range ordered CDW/PLD state in $2H$ -TaSe₂ emerges via a gradual buildup of locally correlated lattice distortions, and not via a spontaneous emerging of uniform lattice distortions at T_{CDW} .

This finding sheds new light on the genesis of CDW/PLDs in low-dimensional solids and prompts further investigations.

The compound $2H$ -TaSe₂ belongs to the widely studied family of transition metal chalcogenides, which, depending on the chemical composition, parent structure type, and temperature, appear in various CDW/PLD states [1, 12–14]. At an atomic level, $2H$ -TaSe₂ may be looked at as a stack of Ta-Se layers held together by weak van der Waals interactions. In a layer, a Ta atomic plane is sandwiched between two hexagonal Se atomic planes, forming strong ionic bonds within a local trigonal-prismatic unit [Fig. 1(f)]. In the high-temperature normal state, $2H$ -TaSe₂ is a bad metal with pseudogap and c -axis resistivity 20–50 times larger than the in-plane resistivity. It undergoes a transition to an incommensurate (I) CDW/PLD phase at $T_{\text{(I)CDW}} \sim 122$ K with a modulation close to a $3a \times 3a$ superstructure followed by another transition into a commensurate (C) $3a \times 3a$ CDW/PLD phase at $T_{\text{(C)CDW}} \sim 90$ K, where a is the plane lattice parameter. Concurrently, a CDW energy gap of ~ 80 meV appears [1, 15–19]. In the CDW/PLD state of $2H$ -TaSe₂, Ta atoms appear displaced from their position in the undistorted hexagonal lattice forming a repetitive pattern of small planar clusters. The in-plane static displacement of Ta atoms has been found to be much larger than that of Se atoms [20–26]. To date, no well-defined lattice distortions have been identified above the temperature of the onset of the first (I)-CDW/PLD phase. However, observed “pseudogap”-like features, strong two-phonon mode in Raman spectra and significant diffuse x-ray scattering near $3a \times 3a$ superstructure reflections indicate that local structural distortions related to the CDW/PLD state are likely to exist at temperatures as high as room temperature [27–34]. We study the distortions by both conventional and resonant high-energy x-ray diffraction (XRD) coupled to atomic pair distribution function (PDF) analysis and reverse Monte Carlo (RMC) simulations in the temperature range from 400 to 100 K, concentrating on the local arrangement of Ta atoms. Fine details of the arrangement

*Corresponding author. petko1vg@cmich.edu

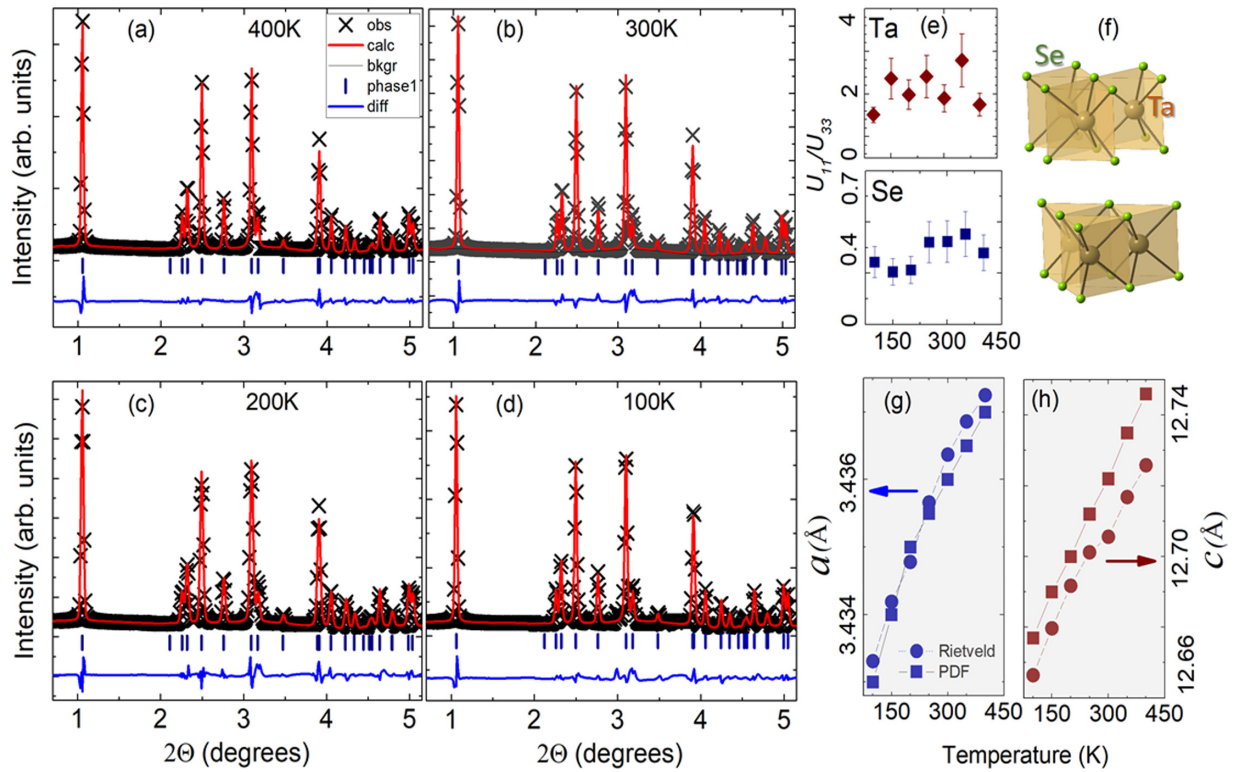


FIG. 1. (a)–(d) Rietveld fit (red line) to high-energy XRD patterns (symbols) for $2H$ -TaSe₂ collected at different temperatures. The residual difference (blue line) is shifted by a constant factor for clarity. (e) Ratio of the anisotropic thermal factors u_{11} and u_{33} for Ta (red rhombuses) and Se (blue squares) atoms obtained by Rietveld analysis. (f) Fragment of the layers of Ta-Se trigonal prisms forming $2H$ -TaSe₂. (g) and (h) Hexagonal lattice parameters a and c for $2H$ -TaSe₂ as a function of temperature obtained by Rietveld (circles) and atomic PDF (squares) analysis.

are well revealed and thoroughly assessed to highlight the important role of local lattice distortions in the temperature-driven formation of the CDW/PLD state of $2H$ -TaSe₂.

A high-quality $2H$ -TaSe₂ sample was provided by 2DSemiconductors [35]. It was subjected to XRD experiments using synchrotron x rays with energy of 105.7 keV ($\lambda = 0.1173$ Å) [36]. Exemplary XRD patterns collected at different temperatures and results from Rietveld fits to the patterns are shown in Figs. 1(a)–1(d). The fits confirm the hexagonal type (space group $P6_3/mmc$) of the average crystal structure of $2H$ -TaSe₂ and also show that its lattice parameters gradually diminish with decreasing temperature [Figs. 1(g) and 1(h)]. Refined thermal factors indicate that the amplitude of the in-plane rms vibrations of Ta atoms is twice that of the out-of-plane vibrations for all studied temperatures. The situation with the displacements of Se atoms is reversed [Fig. 1(e)]. Thus, in line with the findings of prior studies [1,20,24], the results of Rietveld analysis indicate the presence of significant positional disorder of Ta and Se atoms within and between the Ta-Se layers, respectively. Note that, due to their nature, XRD data reflect instantaneous positions of atoms and, hence, the observed disorder may reflect not only static but also possible dynamic rms atomic displacements.

Analysis of total atomic PDFs derived from high-energy XRD patterns provides more clues about the character of that disorder (Fig. 2). In particular, the atomic PDF for $2H$ -TaSe₂ obtained at 400 K may be well approximated

with a model based on structure parameters, including lattice parameters, atomic positions, and rms vibrational amplitudes, obtained by Rietveld analysis of the corresponding XRD pattern [Fig. 2(b)]. The result indicates that, barring the large anisotropy of rms atomic vibrations, the local and average crystal structures of $2H$ -TaSe₂ are similar above room temperature. On the other hand, only the higher- r part of the atomic PDF for $2H$ -TaSe₂ obtained at 100 K, i.e., below T_{CDW} , may be well approximated by Rietveld fit derived structure parameters [Fig. 2(c)]. The observation indicates significant divergence of the local structure of the CDW/PLD state of $2H$ -TaSe₂ from the average hexagonal crystal structure. Analysis of the low- r part of the PDFs indicates that structural features that may not be explained by the average crystal structure appear already at 300 K as a high- and low- r shoulder of the first and second PDF peak, respectively [Fig. 2(d)]. The features become increasingly distinct with decreasing temperature, indicating that, upon cooling below room temperature, the near neighbor distances in $2H$ -TaSe₂ become multimodal.

In particular, the first peak in the PDF for undistorted $2H$ -TaSe₂ would be well defined, reflecting the set of identical distances between Ta atoms centering the perfect trigonal-prismatic units and Se atoms occupying the vertices of the units [Fig. 2(a)]. The units appear increasingly distorted, i.e., different near neighbor Ta-Se distances emerge, as the CDW/PLD state of $2H$ -TaSe₂ is approached on cooling. Furthermore, the second peak in the PDF for undistorted

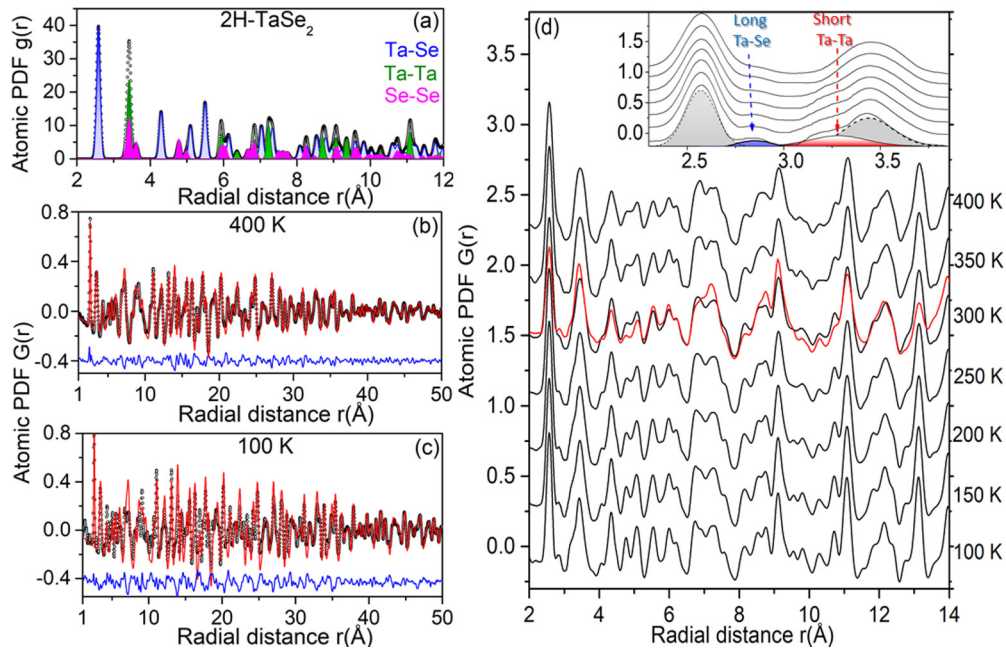


FIG. 2. (a) Computed total (symbols) and partial (colors) atomic PDFs for $2H$ -TaSe₂ showing the overlap of first neighbor Se-Se and Ta-Ta bonding distances in undistorted $2H$ -TaSe₂. (b) and (c) Fits (red line) to the experimental (symbols) total PDFs for $2H$ -TaSe₂ obtained at 400 and 100 K. The residual difference (blue line) is shifted by a constant factor for clarity. The fits are based on a single unit cell model with a $P6/3mmc$ symmetry. The low- r part of the 100 K PDF is poorly reproduced by the average hexagonal structure. (d) Low- r part of experimental total PDFs (black line) for $2H$ -TaSe₂ obtained at different temperatures. Ta-differential PDF (red line) obtained by resonant high-energy XRD is also shown. The first two physical peaks of the total PDFs are shown in the inset. Arrows mark the evolution of peak shoulders reflecting the appearance of unusually long Ta-Se (blue) and short Ta-Ta (red) distances with decreasing temperature. Shaded areas emphasize long Ta-Se (blue), short Ta-Ta (red), and unmodified (black) Ta-Se and Ta-Ta bonding distances. Note that the observed misfit between the local and average structure in (c) and broad distribution of short Ta-Ta distances in (d) are reminiscent of the structural peculiarities exhibited by the CDW state of CeTe₃, where the PLDs involve the formation of an ordered pattern of distinct short and long Te-Te bonds [9].

$2H$ -TaSe₂ would also be well defined, reflecting the equal in length Se-Se and Ta-Ta distances involving atoms from nearby perfect trigonal-prismatic units [Fig. 2(a)]. Unusually short either Ta-Ta or Se-Se distances emerge in $2H$ -TaSe₂ already near room temperature. The distances become more distinct upon cooling, as indicated by the thermal evolution of the low- r shoulder of the second peak in the respective PDFs. To identify these distances, we conducted a resonant high-energy XRD experiment at the K edge of Ta. By its nature, the resulting Ta-differential atomic PDF reflects only structural features involving Ta atoms, that is, Ta-Se and Ta-Ta atomic pair correlations [36,37]. In addition, it doubles the experimental sensitivity to the latter. For reference, the contribution of Ta-Ta atomic correlations to the total and Ta-differential PDFs for $2H$ -TaSe₂ is about 28% and 50%, respectively. Experimental Ta-differential PDF data help identify the low- r shoulder of the second PDF peak as unusually short Ta-Ta bonding distances (Supplemental Material Fig. S3). Evidently, upon cooling below room temperature, some nearby Ta atoms in $2H$ -TaSe₂ come closer together in comparison to the average crystal structure.

To reveal the character of the apparent clustering of Ta atoms, we built large-scale three-dimensional (3D) structure models using RMC [36]. The models were based on a $150 \text{ \AA} \times 150 \text{ \AA} \times 90 \text{ \AA}$ configuration of 80 500 Ta and Se atoms cut out from the hexagonal lattice of $2H$ -TaSe₂. The large size of the model configuration allowed us to explore

Ta-Ta pair correlations well beyond the $3a \times 3a$ repetitive unit of the CDW/PLD state of $2H$ -TaSe₂. The configuration was refined against the total and Ta-differential PDF data obtained at 300 K and a model for the room temperature structure of $2H$ -TaSe₂ was produced. The model was used as an initial guess for the structure of $2H$ -TaSe₂ at 250 K and refined further against the respective PDF data. Following the same approach, we built a sequence of structure models tracking the evolution of local distortions of Ta planes in $2H$ -TaSe₂ upon cooling from above room temperature down towards T_{CDW} , where the first (I)-CDW/PLD phase is formed. The models reproduce the experimental PDF data in very good detail (Fig. S4).

Analysis of the RMC refined models shows that, above 300 K, Ta-Ta bonding distances in $2H$ -TaSe₂ exhibit a broad symmetric distribution centered at about 3.45 \AA , i.e., that the rms displacements of Ta atoms are largely uncorrelated in nature. Clear signatures of correlated Ta displacements, appearing as unusually short Ta-Ta distances, emerge at 300 K. The distances become increasingly distinct with decreasing temperature, forming a pattern characteristic to the small-size clusters of Ta atoms known to exist in the CDW/PLD state of $2H$ -TaSe₂ (FIG. 3). The average value of the short distances is about $3.35(1) \text{ \AA}$ at 100 K [38]. Notably, not all clusters appear perfect at that temperature [Fig. 3(f)]. However, when averaged out over the 3D model structure, they appear consistent with the $3a \times 3a$ superstructure of

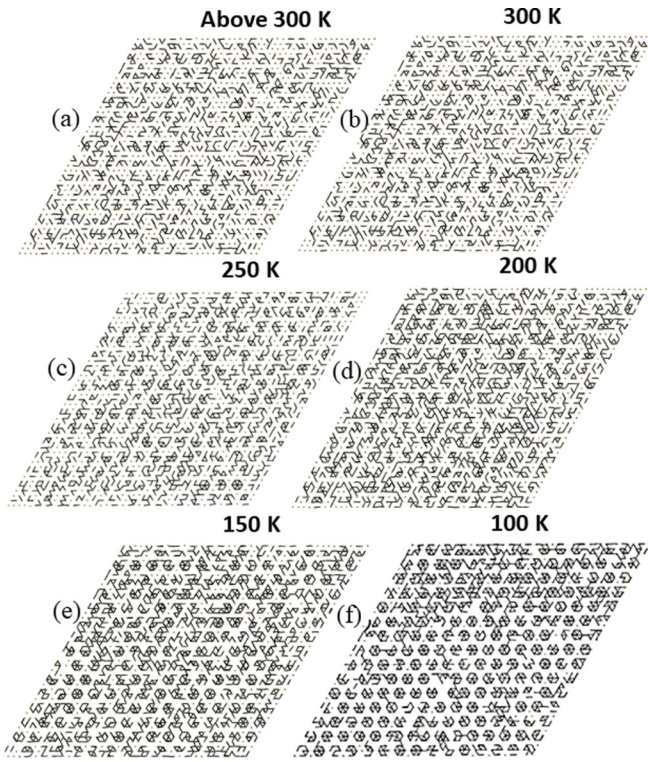


FIG. 3. Top view of $150 \text{ \AA} \times 150 \text{ \AA}$ Ta planes in the 3D structure models for $2H\text{-TaSe}_2$ representing the evolution of local lattice distortions with decreasing temperature. Dark short lines represent Ta-Ta bonding distances shorter than 3.40 \AA . Such distances are present but are orientationally disordered at temperature above 300 K . The distances gradually become both more distinct and correlated with decreasing temperature, eventually forming a periodic pattern at 100 K , i.e., below T_{CDW} . Broken lines in blue and red are a guide to the eye.

hexagons of seven Ta atoms [Fig. 4(a)] suggested by prior experiments [20–27]. Likely because of the imperfections, the underlying crystal lattice appears somewhat distorted, i.e., not quite commensurate with the perfect hexagonal lattice of undistorted $2H\text{-TaSe}_2$ (Fig. S7). Due to the in-plane clustering of Ta atoms and out-of-plane motion of Se atoms, Ta-Se units in the CDW/PLD state of $2H\text{-TaSe}_2$ also appear distorted (Fig. S4) but, as analysis of Se-Ta-Se bond angles shows, their trigonal-prismatic geometry is largely preserved (Fig. S6).

The picture, which emerges for the formation of the superstructure of Ta atoms in the CDW/PLD state of $2H\text{-TaSe}_2$, is therefore as follows (Fig. 3): Ta atoms suffer considerable in-plane positional disorder above room temperature, where thermal excitation effects appear to destroy possible correlations between their displacements. Short Ta-Ta bonds though do exist and are seen to become fairly correlated near room temperature. The correlations remain local with decreasing temperature, leading to the formation of small-size Ta clusters at about 200 K . The clusters become distinct and clearly separated from each other at about 150 K . Likely, that is because they share peripheral atoms with their neighbors, and can no longer sustain a large distribution of Ta-Ta bond lengths/strength upon further cooling. Finally, at 100 K , i.e., below T_{CDW} , the clusters appear arranged in a distinct

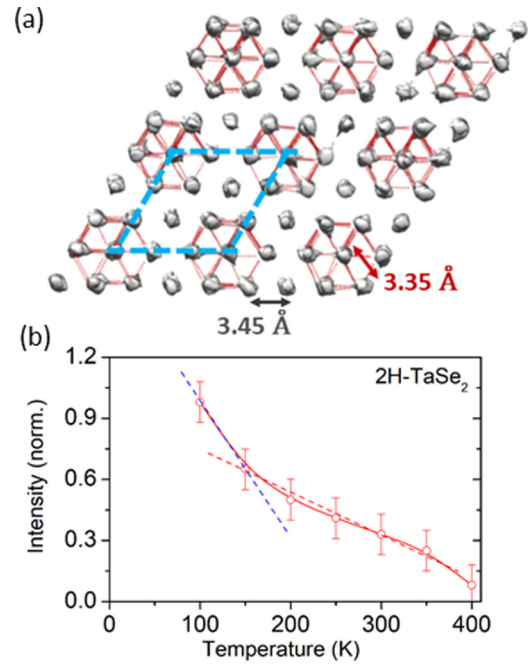


FIG. 4. (a) Top view of a “bulk-averaged” Ta plane in the first CDW/PLD phase of $2H\text{-TaSe}_2$ obtained by mapping the respective 3D model onto a single Ta plane. The $3a \times 3a$ superstructure unit cell of the phase is outlined with a blue line. Red broken lines highlight the presence of hexagon-shaped clusters of Ta atoms. The average distance between Ta atoms at the center and outer part of the clusters is $3.35(1) \text{ \AA}$. The average distance between the latter and atoms that do not belong to the clusters is about $3.45(1) \text{ \AA}$. Irregular gray spheres are contour plots of the bulk-averaged spatial (density) distribution of Ta atoms in the first CDW/PLD phase of $2H\text{-TaSe}_2$, as evaluated from the respective 3D model. For clarity, the contour plots are terminated at density values smaller than 5% of the maximum value. (b) Normalized intensity of the higher- r shoulder of the first peak in the PDF data as a function of temperature (see Fig. S8). The intensity may serve as a “model-independent” parameter describing the temperature-driven evolution of local lattice distortions in $2H\text{-TaSe}_2$ into the $3a \times 3a$ superstructure shown in (a). The evolution is seen to exhibit a kink close to T_{CDW} . The kink may be associated with the crossover between the pseudogap and band-gap regimes in $2H\text{-TaSe}_2$ [32]. Also, it may be associated with the observed kink in the transport properties of $2H\text{-TaSe}_2$ [42].

$3a \times 3a$ periodic superstructure [Fig. 4(a)]. Because the bonding distances between atoms in the clusters remain somewhat different, the clusters are unlikely to be completely aligned with each other, thus leading to a finite average incommensurability of the emerged first CDW/PLD phase (Fig. S7). Upon further cooling the clusters are likely to become near perfect and lock into a commensurate superstructure to minimize the elastic energy [27,33]. Upon a consequent warming/cycling in a narrow temperature range, the array of existing Ta clusters, or different parts of it, may follow a different spatial trajectory and even form multiple transient CDW/PLD phases, as observed by experiment [39–42].

In conclusion, experimental atomic PDF analysis and large-scale 3D structure simulations allow us to reveal the genesis of PLDs in the CDW phase of $2H\text{-TaSe}_2$ in fine detail. We find that Ta atoms undergo significant in-plane rms

displacements seen as unusually short Ta-Ta distances already near room temperature. The amplitude and direction of the displacements above T_{CDW} appear close to those of the static distortions of Ta planes observed below T_{CDW} . The difference is that the latter form a 3D periodic pattern, whereas the former are correlated over short-range distances alone, with the correlation length gradually increasing with decreasing temperature [Fig. 4(b)]. Thus, the transition between the normal and CDW/PLD state of $2H$ -TaSe₂ appears gradual and, in this respect, the locally correlated displacements of Ta atoms above T_{CDW} may be looked at as a precursor of the PLDs below T_{CDW} . Such a relationship may well explain the emergence of a “precursor” CDW pseudogap in the normal state near room temperature and its smooth evolution into a band gap below T_{CDW} [32]. In particular, the pseudogap may

be attributed to the locally correlated Ta displacements and the band gap may be understood as a consequence of the complete alignment of these displacements into a $3a \times 3a$ superstructure. Our findings can also help improve our understanding of CDWs in low-dimensional solids beyond $2H$ -TaSe₂, including streamline theory relating the magnitude of PLDs, CDW energy gap, and T_{CDW} (Fig. S9).

This work was supported by the U.S. Department of Energy, Office of Science, Office of Basic Energy Sciences under Award No. DE-SC0006877 and used resources of the Advanced Photon Source at the Argonne National Laboratory provided by the DOE Office of Science under Contract No. DE-AC02-06CH11357. Thanks are due to O. Shovon for the help with the synchrotron XRD experiment.

-
- [1] K. Rossnagel, *J. Phys. Condens. Matter*, **23**, 213001 (2011).
- [2] X. Zhu, J. Guo, J. Zhang, and E. W. Plummer, *Adv. Phys.:* X **2**, 622 (2017).
- [3] C.-W. Chen, J. Choe, and E. Morrosan, *Rep. Prog. Phys.* **79**, 084505 (2016).
- [4] U. Chatterjee, J. Zhao, M. Iavarone, R. Di Capua, J. P. Castella, G. Karapetkov, C. D. Mallakas, M. G. Kanatzidis, H. Claus, J. P. C. Ruff, F. Weber, J. van Wezel, J. C. Campuzano, R. Osborn, M. Randeria, N. Trivedi, M. R. Norman, and S. Rozenkranz, *Nat. Commun.* **6**, 6313 (2015).
- [5] L. Li, X. Deng, Z. Wang, Y. Liu, M. Abeykoon, E. Dooryhee, A. Tomic, Y. Huang, J. B. Warren, E. S. Bozin, S. J. L. Billinge, Y. Sun, Y. Zhu, G. Kotliar, and C. Petrovic, *npj Quantum Mater.* **2**, 16 (2017).
- [6] Y. Liu, D. F. Shao, L. J. Li, W. J. Lu, X. D. Zhu, P. Tong, R. C. Xiao, L. S. Ling, C. Y. Xi, L. Pi, H. F. Tian, H. X. Yang, J. Q. Li, W. H. Song, X. B. Zhu, and Y. P. Sun, *Phys. Rev. B* **94**, 045131 (2016).
- [7] K. Wijayarathne, J. Zhao, Ch. Malliakas, D. Y. Chung, M. G. Kanatzidis, and U. Chatterjee, *J. Mater. Chem. C* **5**, 11310 (2017).
- [8] S. van Smaalen, *Acta Crystallogr. Sect. A: Found. Adv* **A61**, 51 (2005).
- [9] H. J. Kim, C. D. Malliakas, A. T. Tomic, S. H. Tessmer, M. G. Kanatzidis, and S. J. L. Billinge, *Phys. Rev. Lett.* **96**, 226401 (2006).
- [10] T. Egami and S. J. L. Billinge, *Underneath the Bragg Peaks: Structural Analysis of Complex Materials* (Pergamon, Oxford, England, 2003).
- [11] V. Petkov, *Characterization of Materials* (Wiley, New York, 2003).
- [12] M. Kertesz and R. Hoffmann, *J. Am. Chem. Soc.* **106**, 3453 (1984).
- [13] C. Rovira and M.-H. Whangbo, *Inorg. Chem.* **32**, 4094 (1993).
- [14] A. Meetsma, G. A. Wiegers, R. J. Haange, and J. L. de Boer, *Acta Crystallogr. Sect. C: Struct. Chem.* **46**, 1598 (1990).
- [15] H. Luo, W. Xie, J. Tao, H. Inoe, A. Gyenis, J. W. Krizan, A. Yazdani, Y. Zhu, and R. J. Cava, *Proc. Natl. Acad. Sci. USA* **112**, E1174 (2015).
- [16] T. Ritschel, J. Trinckauf, K. Koepf, B. Buchner, M. v. Zimmermann, H. Berger, Y. I. Joe, M. Abbamonte, and J. Geck, *Nat. Phys.* **11**, 328 (2015).
- [17] M. Kratochvilova, A. D. Hiller, A. R. Wildes, L. Wang, S.-W. Cheong, and J.-G. Park, *npj Quantum Mater.* **2**, 42 (2017).
- [18] D. C. Miller, S. D. Mahanti, and P. M. Duxbury, *Phys. Rev. B* **97**, 045133 (2018).
- [19] W. Wang, D. Dietzel, and A. Schirmeisen, *Sci. Rep.* **9**, 7006 (2019).
- [20] D. E. Moncton, J. D. Ake, and F. J. DiSalvo, *Phys. Rev. B* **16**, 801 (1977).
- [21] R. M. Fleming, D. E. Moncton, D. B. McWhan, and F. J. DiSalvo, *Phys. Rev. Lett.* **45**, 576 (1980).
- [22] T. Butz, S. Saibene, and A. Lerf, *J. Phys. C: Solid State Phys.* **19**, 2675 (1986).
- [23] R. Brower and F. Jellinek, *Physica B+C* **99**, 51 (1980).
- [24] R. M. Fleming, D. E. Moncton, J. D. Axe, and G. S. Brown, *Phys. Rev. B* **30**, 1877 (1984).
- [25] J. van Landuyt, G. van Tendeloo, and S. Amelinckx, *Phys. Status Solidi A* **26**, 359 (1974).
- [26] J. van Landuyt, G. A. Wiegers, and S. Amelinckx, *Phys. Status Solidi A* **46**, 479 (1978).
- [27] J. Dai, E. Calleja, J. Alldredge, X. Zhu, L. Li, W. Lu, Y. Sun, T. Wolf, H. Berger, and K. McElroy, *Phys. Rev. B* **89**, 165140 (2014).
- [28] D. S. Inosov, D. V. Evtushinsky, V. B. Zabolotnyy, A. A. Kordyuk, B. Buchner, R. Follath, H. Berger, and S. V. Borisenko, *Phys. Rev. B* **79**, 125112 (2009).
- [29] R. L. Barnett, A. Polkovnikov, E. Demler, W.-G. Yin, and W. Ku, *Phys. Rev. Lett.* **96**, 026406 (2006).
- [30] S. Sugai, K. Murase, S. Uchida, and S. Tanaka, *J. de Phys. Colloq.* **42(C6)**, 728 (1981).
- [31] H. M. Hill, S. Chowdhury, J. R. Simpson, A. F. Rigosi, D. B. Newell, H. Berger, F. Tavazza, and A. R. Hight Walker, *Phys. Rev. B* **99**, 174110 (2019).
- [32] S. V. Borisenko, A. A. Kordyuk, A. N. Yaresko, V. B. Zabolotnyy, D. S. Inosov, R. Schuster, B. Büchner, R. Weber, R. Follath, L. Patthey, and H. Berger, *Phys. Rev. Lett.* **100**, 196402 (2008).
- [33] Ph. Leininger, D. Chernyshov, A. Bosak, H. Berger, and D. S. Inosov, *Phys. Rev. B* **83**, 233101 (2011).
- [34] J. Laverock, D. Newby, Jr., E. Abreu, R. Averitt, K. E. Smith, R. P. Singh, G. Balakrishnan, J. Adell, and T. Balasubramanian, *Phys. Rev. B* **88**, 035108 (2013).
- [35] <http://www.hqgraphene.com/TaSe2.php>.

- [36] See Supplemental Material at <http://link.aps.org/supplemental/10.1103/PhysRevB.101.121114> for supporting experimental and computational details.
- [37] V. Petkov, S. Shastri, J.-Woo Kim, S. Shan, J. Luo, J. Wu, and Ch.-J. Zhong, *Acta Crystallogr. Sect. A: Found. Adv.* **74**, 553 (2018).
- [38] Shrinking of Ta-Ta bonds in the order of 0.1 Å is reported by C. B. Scruby, Ph.D. thesis, University of London, 1976, p. 252, <https://spiral.imperial.ac.uk/handle/10044/1/22483>.
- [39] J. E. Inglesfield, *Physica B+C* **99**, 238 (1980).
- [40] M. D. Johannes and I. I. Mazin, *Phys. Rev. B* **77**, 165135 (2008).
- [41] T.-R. T. Han, F. Zhou, Ch. D. Malliakas, P. M. Duxbury, S. D. Mahanti, M. G. Kanatzidis, and Ch.-Y. Ruan, *Sci. Adv.* **1**, e1400173 (2015).
- [42] V. Vescoli, L. Degiorgi, H. Berger, and L. Forró, *Phys. Rev. Lett.* **81**, 453 (1998).